Influence of galaxy rotation and outflows in the Lyman Alpha spectral line

Maria Camila Remolina Gutiérrez

A monograph presented for the degree of
Physicist

Departamento de Física
Facultad de Ciencias
Universidad de los Andes
Colombia

November, 2015

Dedicated to

Someone here

Influence of galaxy rotation and outflows in the Lyman Alpha spectral line

Maria Camila Remolina Gutiérrez

Submitted for the degree of Physicist
November, 2015

Abstract

Your abstract here Your abstract here

Declaration

The work in this monograph is based on research carried out at the Physics Department of Universidad de los Andes, Colombia. No part of this thesis has been submitted elsewhere for any other degree or qualification and it is all my own work unless referenced to the contrary in the text.

Acknowledgements

We acknowledge Alvaro Orsi and Julian Mejia for collaborating with us offering their time, advice and especially data. We used their outflow simulations in order to get our results in the appendix.

Most of our code benefits from the work of the IPython and Matplotlib communities ([1, 2]).

The data, source code and instructions to replicate the results of this paper can be found on `https://github.com/mariacamilaremolinagutierrez/LymanAlpha/`.

MISSING:

- More acknowledgments.

Contents

Chapter 1

Introduction

1.1 The Lyman Alpha emission line

The Lyman Alpha (Ly-α) emission line is the spectral line produced by an excited hydrogen atom when its electron jumps from the second energy level to the first one. This fall causes an emission of a photon with a corresponding wavelenght of 1215.67 $\mathring{A}$. The whole Lyman series was discovered in 1906 by the American physicist Theodore Lyman.

The derivation from this series comes from Niels Bohr's model in which the energy of each level is given by Eq. 1.1.1; where m and e are the mass and charge of the electron, respectively, ϵ_0 is the vacuum permittivity, $\hbar$ is the reduced Planck constant and n is the level.

$$E_n = -\frac{me^4}{2(4\pi\epsilon_0\hbar)^2}\frac{1}{n^2} \tag{1.1.1}$$

When the electron falls from one energy level to the other, it emits a photon with a certain wavelength, determined by Eq. 1.1.2; where h is the Planck constant, c is the speed of light, E_i is the energy at the initial level i and E_f is the energy at the final level f.

$$\lambda = \frac{hc}{E_i - E_f} \tag{1.1.2}$$

For the Lyman series the final level is always $n = 1$, and for the Ly-α line, the initial level is $n = 2$. After plugging this numbers, a wavelength of $1215.67\mathring{A}$ is obtained. This will be the transition we're interested in.

In 1967 Partridge et al. [3] predicted that young galaxies would have a strong Ly-α emission. Nowadays galaxies selected using the Ly-α line are known as Lyman Alpha Emitters (LAEs). Since the first observed LAE by Djorgovski et al. [4] different teams have observed several LAEs ([5], [6], [7], [8], [9], [10], [11], [9], [12], [13], [14], [15], [16], [17]) specially at $z \geq 2$ since it is when the line is redshifted into the optical regime. LAEs became then a tool to explore the extragalactic Universe and with upcoming telescopes such as the James Webb Space Telescope, new ones are going to be discovered with a better resolution and at higher redshifts. This creates a clear motivation to model them and observe them.

As for motivation, these observations have a direct impact in studying the reionization epoch ([18]), properties of the interstellar medium (ISM) and the intergalactic medium (IGM) ([19], [20]), constraining star formation rates of high redshift galaxies, understanding galaxy luminosity functions ([21]) and studying the large scale structure of the Universe. In all of these studies, an understanding of the processes that model the morphology and radiate transfer process behind the Ly-α line, is required. To fully understand the observed spectra of the LAEs, these galaxies must be modeled.

1.2 Existing models of Lyman Alpha Emitters

The resonant nature of the Ly-α line makes modelling it a challenging task, but constraining the nature of LAEs using the line is a common and strong objective.

Analytical solutions for the outcoming spectra in simple ISM static geometries have been derived ([22], [23], [24], [25]). Radiative transfer codes ([20], [26], [27], [28]) have been developed in order to understand the effect of the gas kinematics in the Ly-α line. Special attention have been devoted to the effects of clumpy media ([29]) and expanding/contracting shell/spherical geometries started to be studied ([30], [27], [25]). Hydrodynamic simulations have studied the outcomming spectra of LAEs in large scale simulations [31]. Escape of Ly-α photons at the line center is also a proposed model that fits the observations in a more accurate way ([32], [33], [34]). And Monte Carlo codes have been used in hydrodynamic simulations to study in detail individual galaxies ([26], [35], [36], [37]).

Special attention have been devoted to model the presence of outflows in these galaxies, motivated by previous observational studies. Outflows are a consequence of the interstellar medium (ISM) being ejected from the galaxy due to supernova explosions. Here different models have attempt to simulate more realistic situations involving shell models and cavities ([38]). Blue wings and bumps have been modeled when the outflows regulating the escape of Ly-α photons are still engulfed within a static interstellar medium ([39]). Verhamme et al. [27] created an expanding shell model that despite its geometric simplicity, has been able to fit several Ly-α profiles including: observational, as the ones studied by Hashimoto et al. [40] who reproduced the sources Ly-α lines and calculated their outflow velocities, and simulated, as the ones created by Gronke et al. [41] who determined if degeneracies exist between the different shell model parameters. Also, Orsi et al. [42] creates a wind shell model that could be interpreted as an expanding sphere. Rivera-Thorsen et al. [43] found that no one single effect dominates in governing Ly-α radiative transfer and escape, and that Ly-α peak velocities are consistent with a simple model of an intrinsic emission line overlaid by a blueshifted absorption profile from the outowing wind.

Despite the fact that outflows have been broadly studied, rotation should also be present in these galaxies. Recently, a rotation model, created by Garavito et al. [33] models a rotating spherical galaxy with homogeneous gas mixture and analyzes

that impact in the Ly-α line. However not a lot of attention has been payed to this effect in LAEs.

The joint effect of the above properties should have a direct impact on the morphology of the Ly-α line. This is the subject of this work.

1.3 Radiative Transfer Code

A radiative transfer process is a "physical phenomenon of energy transfer in the form of electromagnetic radiation. The propagation of radiation through a medium is affected by absorption, emission and scattering processes." ([44]). This phenomenon is described by the equation of radiative transfer, Eq. 1.3.3; where I_ν is the spectral radiance, Ω is the solid angle, $k_{\nu,s}$ is the scattering cross section, $k_{\nu,a}$ is the absorption cross section, and j_ν is the emission coefficient. ([45])

$$\frac{1}{c}\frac{\partial}{\partial t}I_\nu + \hat{\Omega}\cdot\nabla I_\nu + (k_{\nu,s}+k_{\nu,a})I_\nu = j_\nu + \frac{1}{4\pi c}k_{\nu,s}\int_\Omega I_\nu d\Omega \tag{1.3.3}$$

The radiative transfer phenomenon describes, among several physical processes, the scattering of a photon in a LAE that has to pass through the galaxy while being absorbed and re-emitted until it escapes. This effect is the one we are interested in. However, analytic solutions for the previous equation have not been derived for non-simple cases, and for this particular situation numerical methods, achieved through computation, are required.

This problem creates a motivation for radiative transfer codes to be implemented. In this monograph a modified version of the code CLARA (Code for Lyman Alpha Radiation Analysis) made by [28] will be used. The code works as follows.

We propose a simplified model in which the galaxy is modeled as an sphere, a homogeneous mixture of dust and hydrogen, undergoing solid-body rotation and

that is expanding in the radial direction due to outflows. There is a central emission in the galaxy of a large number ($\sim$ 100000) of photons. In CLARA, one by one, each photon starts in a random direction in the xyz plane with the natural Ly-α frequency. It continues that path until it encounters a hydrogen atom that absorbs it. It is then re-emitted in another direction and with a different frequency that depends of the velocity, both radial and tangential, of the atom. As there is no dust present in the simulation, the photon is never absorbed by it and continues in this random walk until it escapes from the galaxy. At each point of the walk, CLARA tracks the photon's position, direction and frequency. The final output is a table of these final values for each photon.

1.4 Monograph Overview

This paper is structured as follows. In Chapter 2 we explain in detail the model of rotation and outflow that we use. In Chapter 3 we present the results of our model, specially how the morphology of the line changes with the free parameters. In Chapter 4 we compare our results with a recent observation of a LAE. In the latest Chapter, 5 we present our conclusions and possible future work. Finally, in the Appendix, we present the results of a Ly-α modeled only with the rotation analytical solution by Garavito et al. [33] that then is filtered by a Verhamme et al. [27] expanding shell.

Chapter 2

Model

We use the simplified rotation model developed by [33] in which a rotating galaxy is modeled as a solid rotating sphere, with a homogeneous mixture of hydrogen and dust. There is also the radial expanding velocity. Photons are initially at the center of the sphere. These two velocities are added by components as follows. The equations governing this movement in which the axis of rotation is defined to be align with the z-axis are:

$$v_x = \frac{x}{R} v_{\text{out}} - \frac{y}{R} v_{\text{rot}}, \tag{2.0.1}$$

$$v_y = \frac{y}{R} v_{\text{out}} + \frac{x}{R} v_{\text{rot}}, \tag{2.0.2}$$

$$v_z = \frac{z}{R} v_{\text{out}}, \tag{2.0.3}$$

Where R is the radius of the sphere. The minus/plus sign in the x/y-component of the rotation velocity part indicates the direction of rotation. In this case we take the angular velocity in the same direction as the $\hat{k}$ unit vector.

Now, we'll describe the radiative transfer process that is simulated by the code. Each photon is emitted with the natural Ly-α frequency from the center of the galaxy. The individual scattering of the emitted photon is tracked through a 3D distribution of neutral Hydrogen. The frequency of the photon and its direction of propagation change at every encounter due to the peculiar velocities of the Hydrogen absorbing it and re-emitting it. Once the photon escape the galaxy, its final values are stored: position, direction of propagation, frequency and number of scatterings. For each simulation a histogram of this final frequencies is created and it represents the Ly-α associated to the initial configuration.

We express a photon's frequency in terms of the dimensionless variable:

$$x \equiv (\nu - \nu_a)/\Delta\nu_{\rm D} \tag{2.0.4}$$

Where $\nu_\alpha = 2.46\times10^{15}$ Hz is the Lyα resonance frequency, $\Delta\nu_{\rm D} \equiv \nu_\alpha\sqrt{2kT/m_pc^2} \equiv \nu_a v_{\rm th}/c$ is the Doppler broadening of the line which depends on the neutral gas temperature T or equivalently the thermal velocity $v_{\rm th}$ of the atoms. For the temperature $T = 10^4$K used in our radiative transfer calculations the thermal velocity is $v_{\rm th} = 12.8\,{\rm km\ s^{-1}}$.

2.1 Galaxy Parameters

Our aim is to provide a realistic baseline to compare against observations of LAEs at $z \sim 3$. It has been found by analysis of the abundance and angular correlation function that LAEs reside in DM halos of masses in the range $10^{10} - 10^{11}{\rm M}_\odot$[46]. This mass range corresponds to maximum circular velocities in the range $60 - 125\,{\rm km\ s^{-1}}$and a median halo scale radius of 15kpc. [1].

[1]These results were found using the N-body data available in `www.cosmosim.org`

These galaxies have gas fractions close to 20% ([47]). We approximate that the hydrogen content is 20% the total baryonic content from the cosmological baryon to dark matter abundances $\Omega_b/\Omega_{dm} = 0.1825$ ([48]), multiplied by a primordial Hydrogen fraction of 0.75. All these considerations gives us hydrogen masses in the range $2.7 \times 10^8 - 2.7 \times 10^9 \mathrm{M}_\odot$.

These choices give us a range for the number density of Hydrogen atoms of $4 \times 10^{-4} - 4 \times 10^{-3}$ atoms cm^{-3}. With a Lyman-α cross section at the line center of $\sigma_H = 1.0 \times 10^{-14}$ cm^2 we finally obtain that the optical depth from the cloud's center should be in the range $\tau_{\mathrm{H}} = 2 \times 10^5 - 2 \times 10^6$.

In order to be able to tell the influence of the rotation and outflows velocities in the Ly-α line morphology, a mapping of them is made without concerning of their physical meaning at first, this constitutes the 1st run. In the second run the interesting ranges are identified and narrowed. In the 3rd and last run, the final physical and relevant combinations are made.

All of the selected values with its corresponding run are registered in Tab. 2.1. The way to read it is: for the i^{th} run, all of the permutations of τ_{H} , v_{rot} and v_{out} are run.

RUN	$\mathbf{1}^{st}$	$\mathbf{2}^{nd}$	$\mathbf{3}^{rd}$
τ_{H}	5, 6, 7	5, 6, 7	5, 6
v_{rot} (km s^{-1})	0, 100, 200 ,300	50, 100	50, 100
v_{out} (km s^{-1})	100, 200, 300	25, 50, 75	5, 10, 15, 20

Table 2.1: **Combinations of values in each run.**

Is important to note that if we stand next to the galaxy, not all of the photons emitted are going to be observed because some will have directions that could never reach our position. For this reason, it is very important to define viewing angle so that only photons that escape within that range are counted in the spectrum. As seen in Fig. 2.1, only the photons with escaping direction angle θ respect to the rotation axis that belongs to the range $[\theta_{min} - \theta_{max}]$ will be reach the observer.

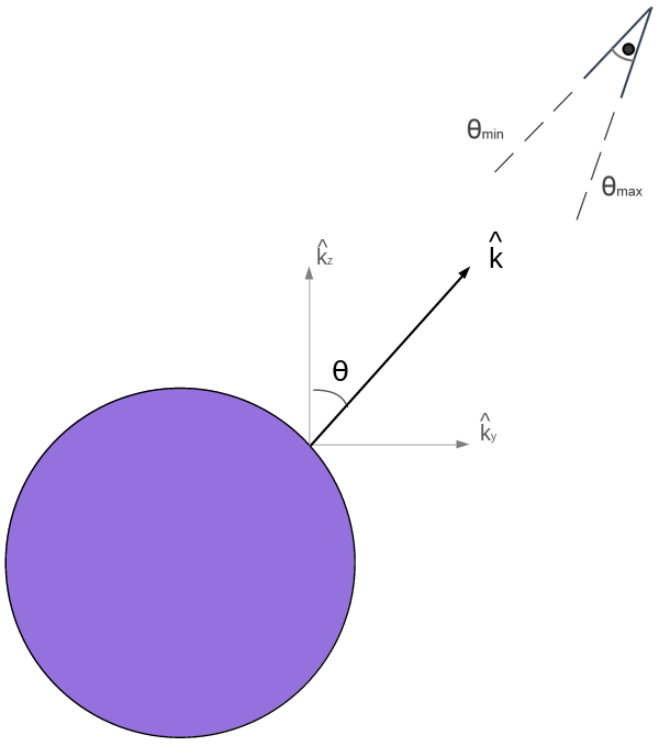

Figure 2.1: **Viewing Angle Sketch:** The galaxy is in the $y-z$ plane perspective and the eye is located at an specific viewing angle of the sphere. Only photons with a direction that enters in his range of vision can enter to the result.

This creates 2 new parameters, the azimuthal angle and the polar angle. However, the galaxy's movement is symmetrical respect to its rotation axis, which implies that the resulting spectrum will not vary depending on the azimuthal angle. This lets us then take all of the photons with azimuthal viewing angle from 0 to 2π for each selected polar range, which we will do for statistical reasons. Regarding the polar angle, we will take spectra from 9 different ranges from 0 to π that are uniform in $\cos(\theta)$ and analyze the influence of this effect as well. All of these results will be seen in the next chapter.

Chapter 3

Results

3.1 Influence of the viewing angle θ

As stated in the preceding chapter, we will also take into account the viewing angle of the galaxy to create the resulting spectra. So in order to proceed we will start stating the influence of this extra parameter in the Ly-α line.

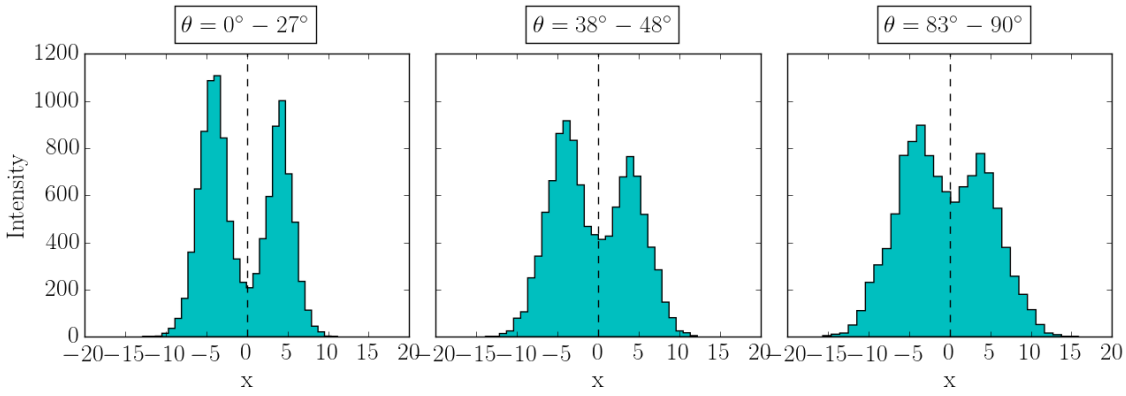

Figure 3.1: **Ly-α profile for different θ:** With $\tau_{\mathrm{H}} = 10^5$, $v_{\mathrm{rot}} = 50$ km s^{-1}and $v_{\mathrm{out}} = 20$ km s^{-1}.

It was noticed that for all of the different combinations that we ran, the effect of θ is always the same. For this, in order to exemplify we will use the particular case of $\tau_{\mathrm{H}} = 10^5$, $v_{\mathrm{rot}} = 50$ km s^{-1}and $v_{\mathrm{out}} = 20$ km s^{-1}. As seen in Fig. 3.1 it is really clear that the intensity of the valley between the two peaks is increased along with θ. This causes an intensity decrease in the rest of the frequencies, thus a broadening

of the line.

Now, as the effect of the viewing angle is understood we can work from now on with a particular range of θ to decrease the number of cases. We ensure the reader it is an analogous behavior for all of them. In particular we will choose the range in which we see the galaxy's angular momentum vector going perpendicular to our relative position vector. In numbers this means: $\theta \in [83°, 96°]$

3.2 Runs

Now, for each of the runs made we will explain how we narrowed our parameter space to obtain our final results. In all of the plots v_{rot} increases in the row from left to right and v_{out} increases in the column from top to bottom.

3.2.1 1st run

In the 1st run we were focused on understanding what each parameter did to the line, more than its physical possibility to be present. For this we chose the values in the second column of Tab. 2.1. The obtained results are in Fig. 3.2 3.3 and 3.4.

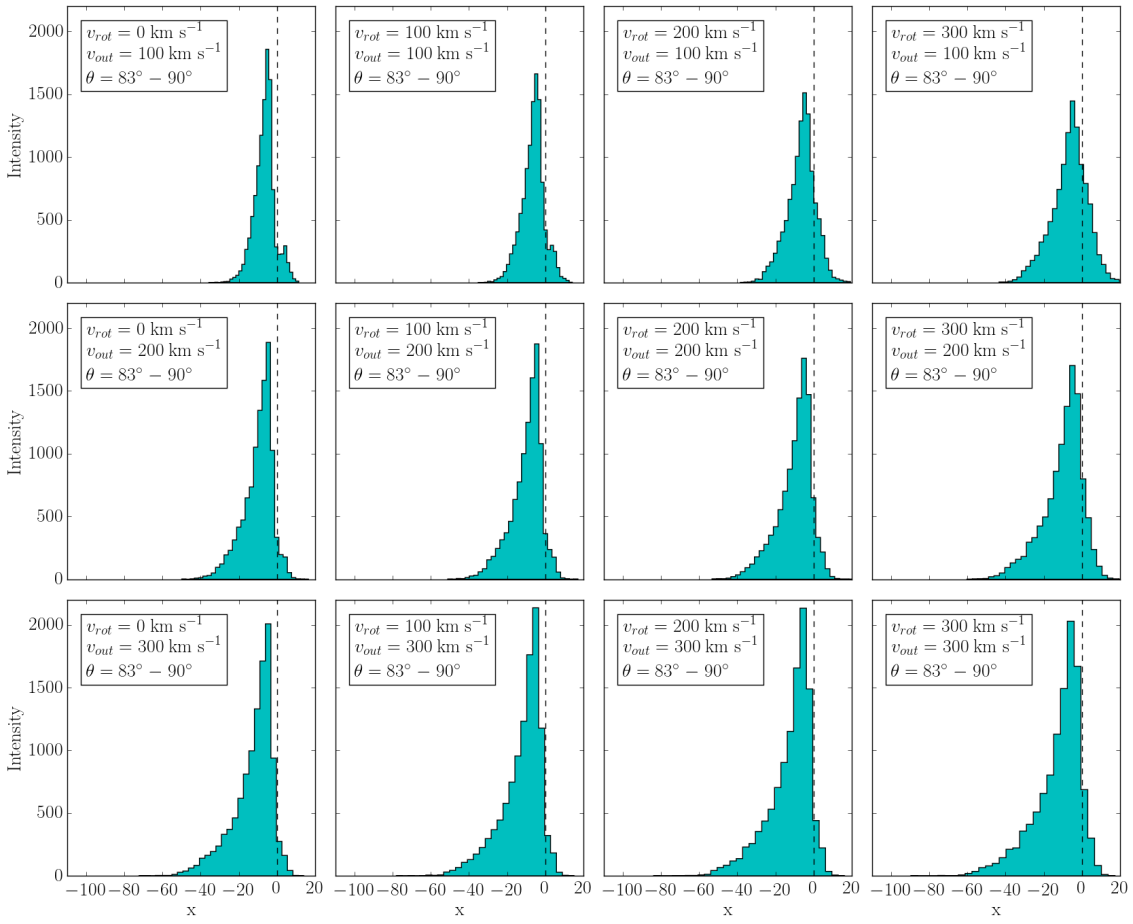

Figure 3.2: **Ly-α profile for $\tau_{\mathrm{H}} = 10^5$:** With v_{rot} ranging $0, 100, 200, 300$ km s^{-1}and v_{out} ranging $100, 200, 300$ km s^{-1}.

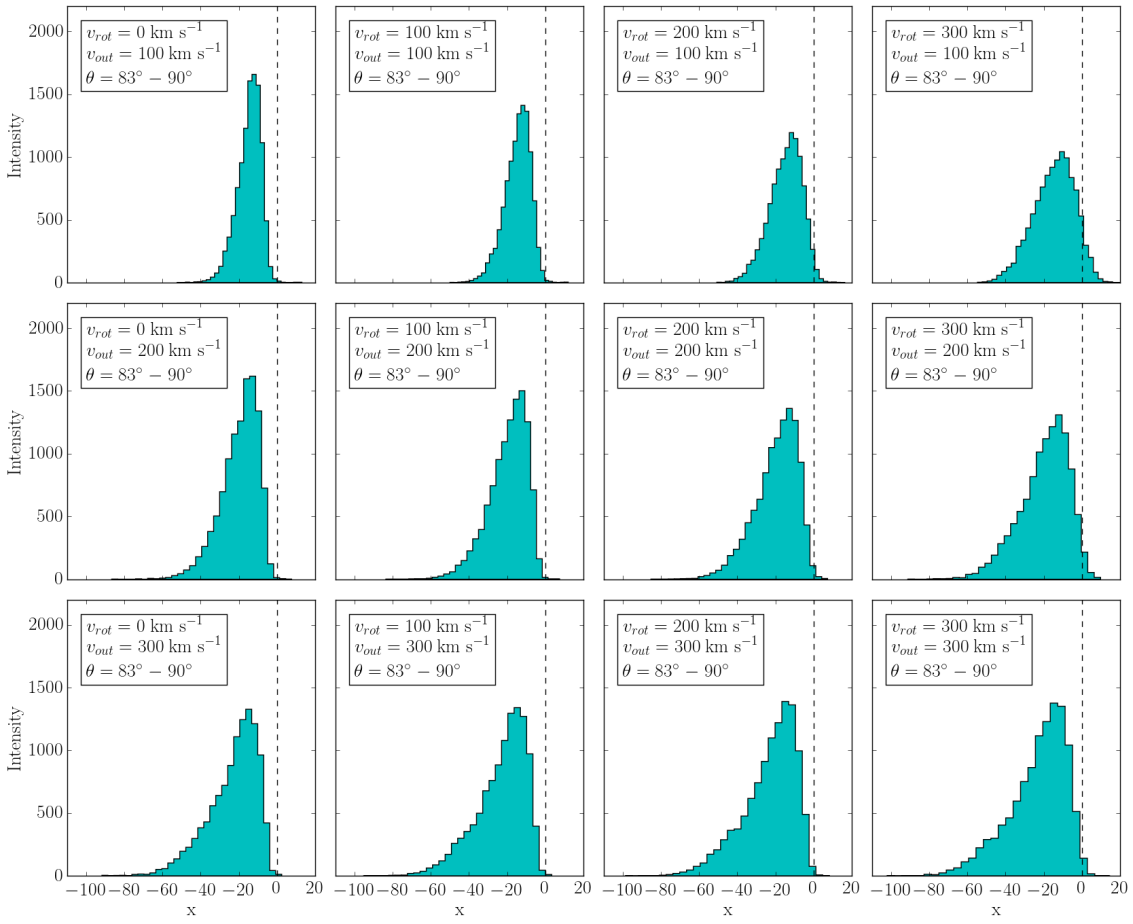

Figure 3.3: **Ly-α profile for $\tau_{\mathrm{H}} = 10^6$:** With v_{rot} ranging $0, 100, 200, 300$ km s^{-1}and v_{out} ranging $100, 200, 300$ km s^{-1}.

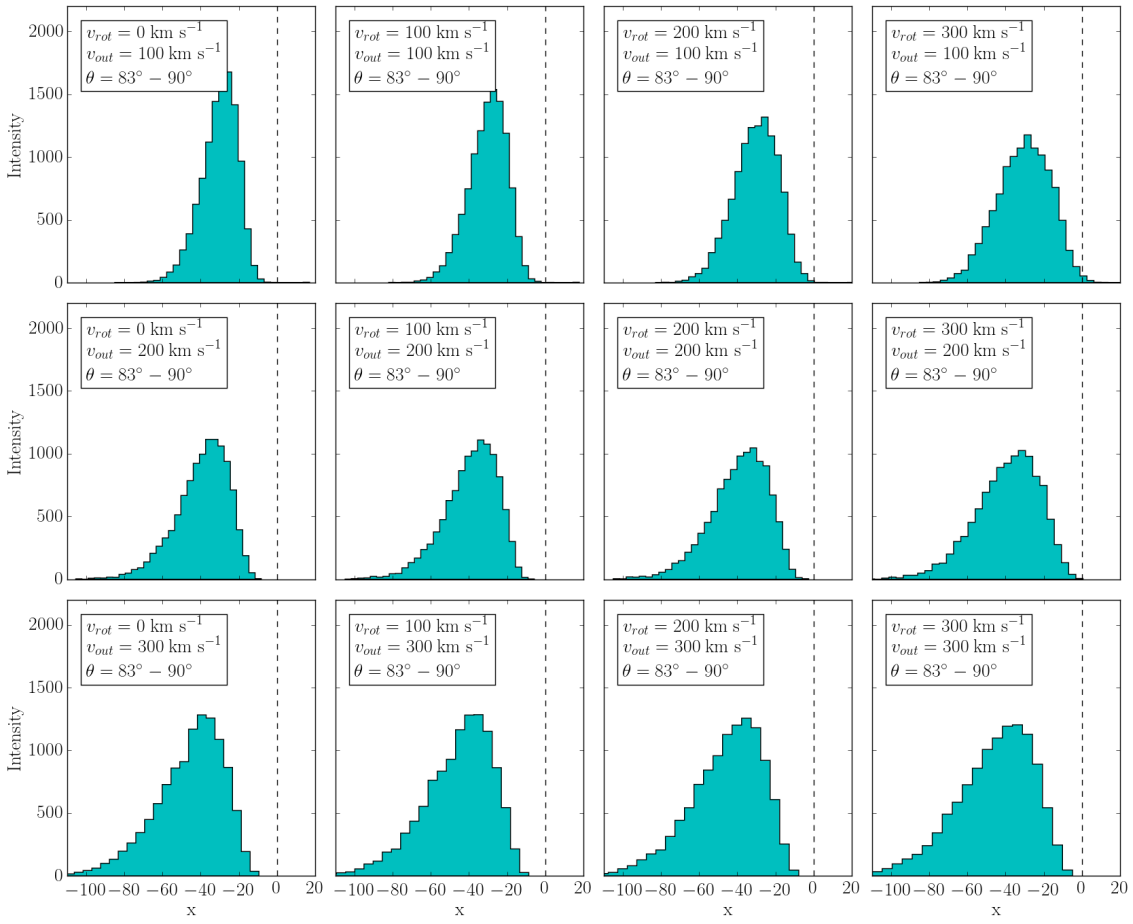

Figure 3.4: **Ly-α profile for $\tau_{\rm H} = 10^7$:** With $v_{\rm rot}$ ranging $0, 100, 200, 300$ km s^{-1}and $v_{\rm out}$ ranging $100, 200, 300$ km s^{-1}.

In these three sets of figures (Fig. 3.2 3.3 3.4) it is noted that most of the lines are a single peaks. However the effect of rotation should create two. Only in few squares the 2 peaks are visible but they are almost insignificant in comparison and there has to be low $v_{\rm rot}$ and $v_{\rm out}$ to obtain them. This means that the outflows effect so much larger than the other one, and in order to compare the influence of both is necessary to lower $v_{\rm out}$. That is the purpose of the 2nd run.

3.2.2 2nd run

In this run, the velocities were narrowed and much more physical parameters were selected. This last constrain means that the velocities are now consistent with the LAE's mass and typical properties. However the $v_{\rm out}$ is still relatively big compared to the $v_{\rm rot}$.

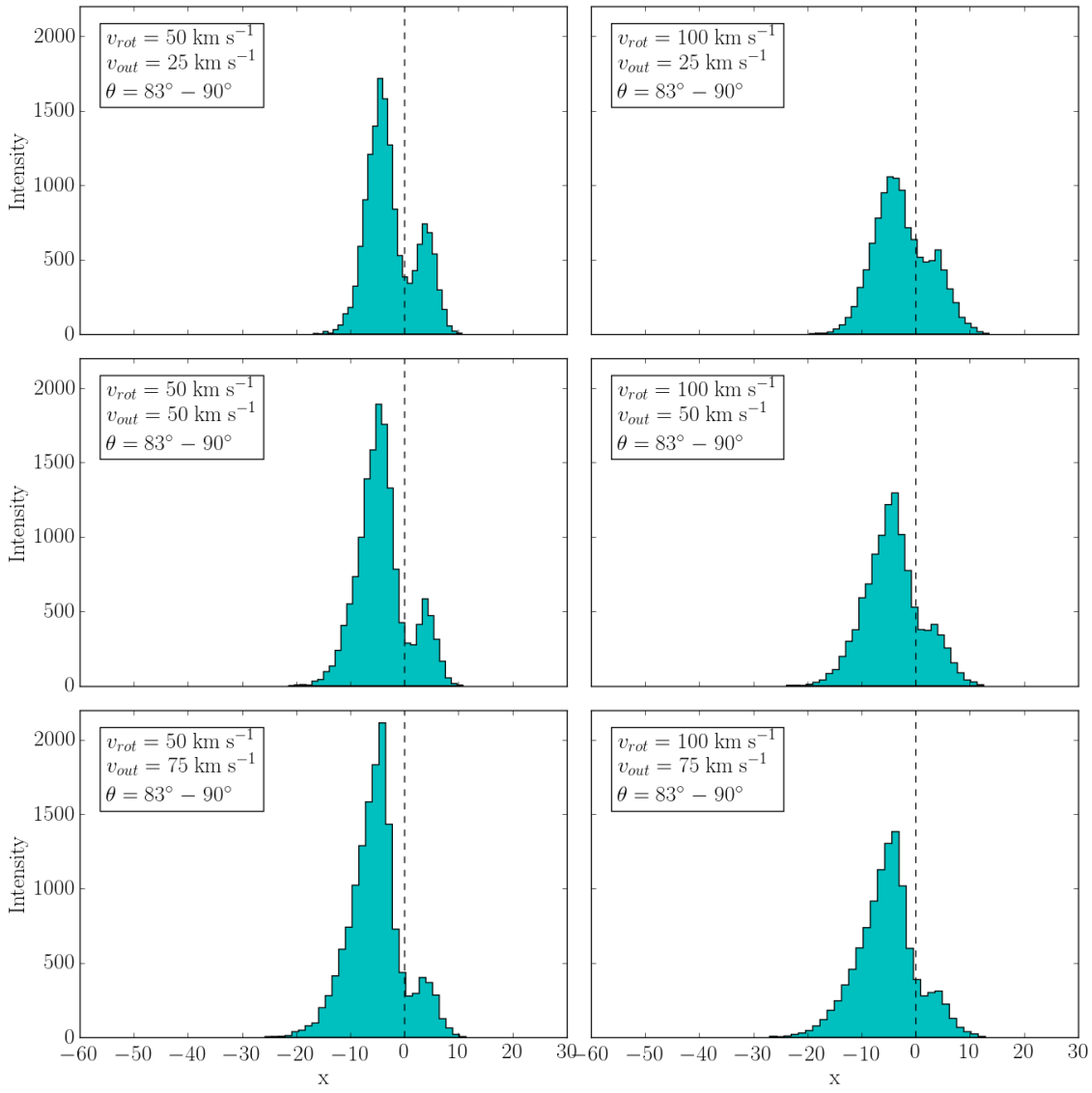

Figure 3.5: **Ly-α profile for $\tau_{\rm H} = 10^5$:** With $v_{\rm rot}$ ranging $50, 100$ km s^{-1}and $v_{\rm out}$ ranging $25, 50, 75$ km s^{-1}.

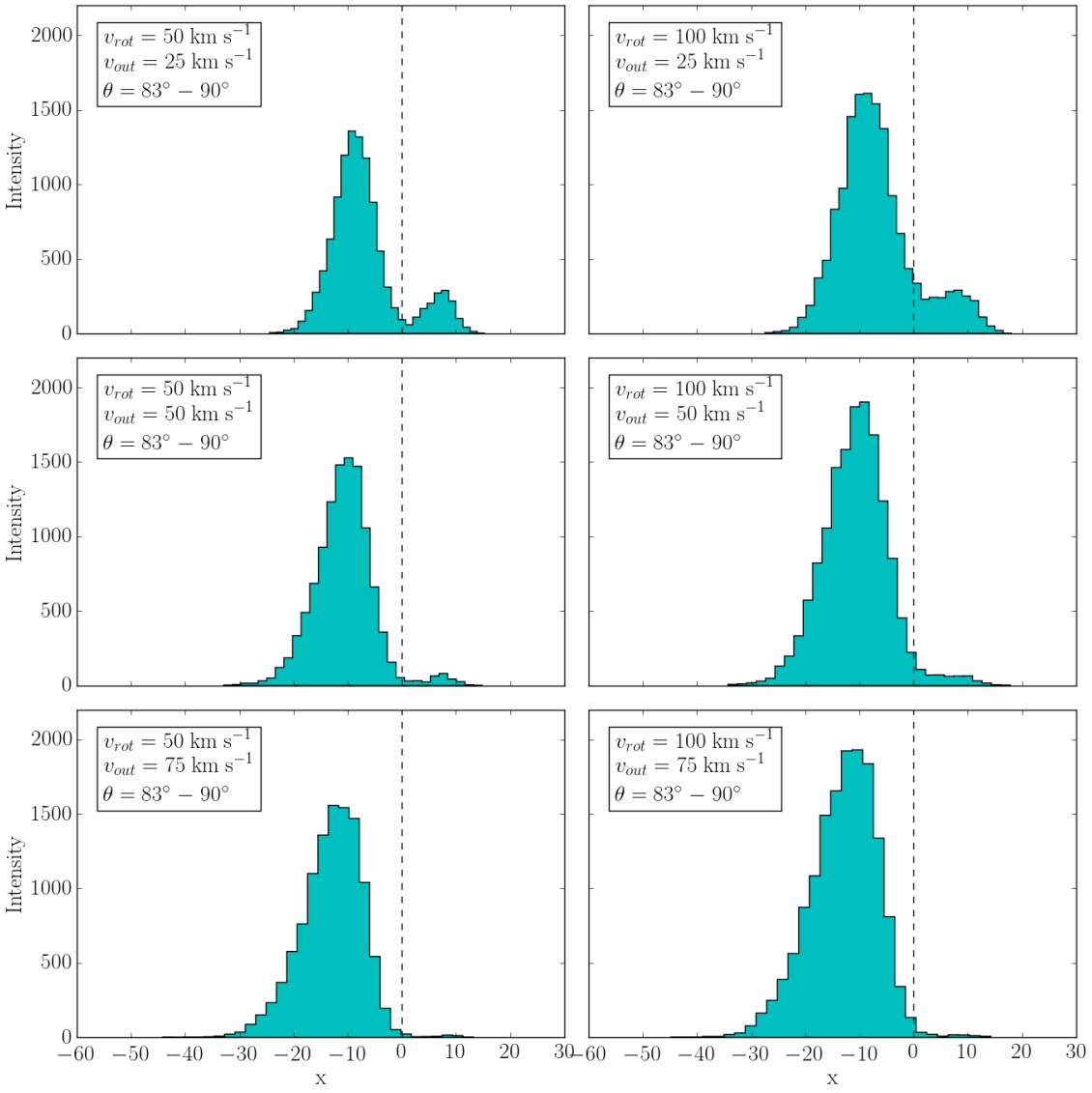

Figure 3.6: **Ly-α profile for $\tau_{\rm H} = 10^5$:** With $v_{\rm rot}$ ranging $50, 100$ km s^{-1}and $v_{\rm out}$ ranging $25, 50, 75$ km s^{-1}.

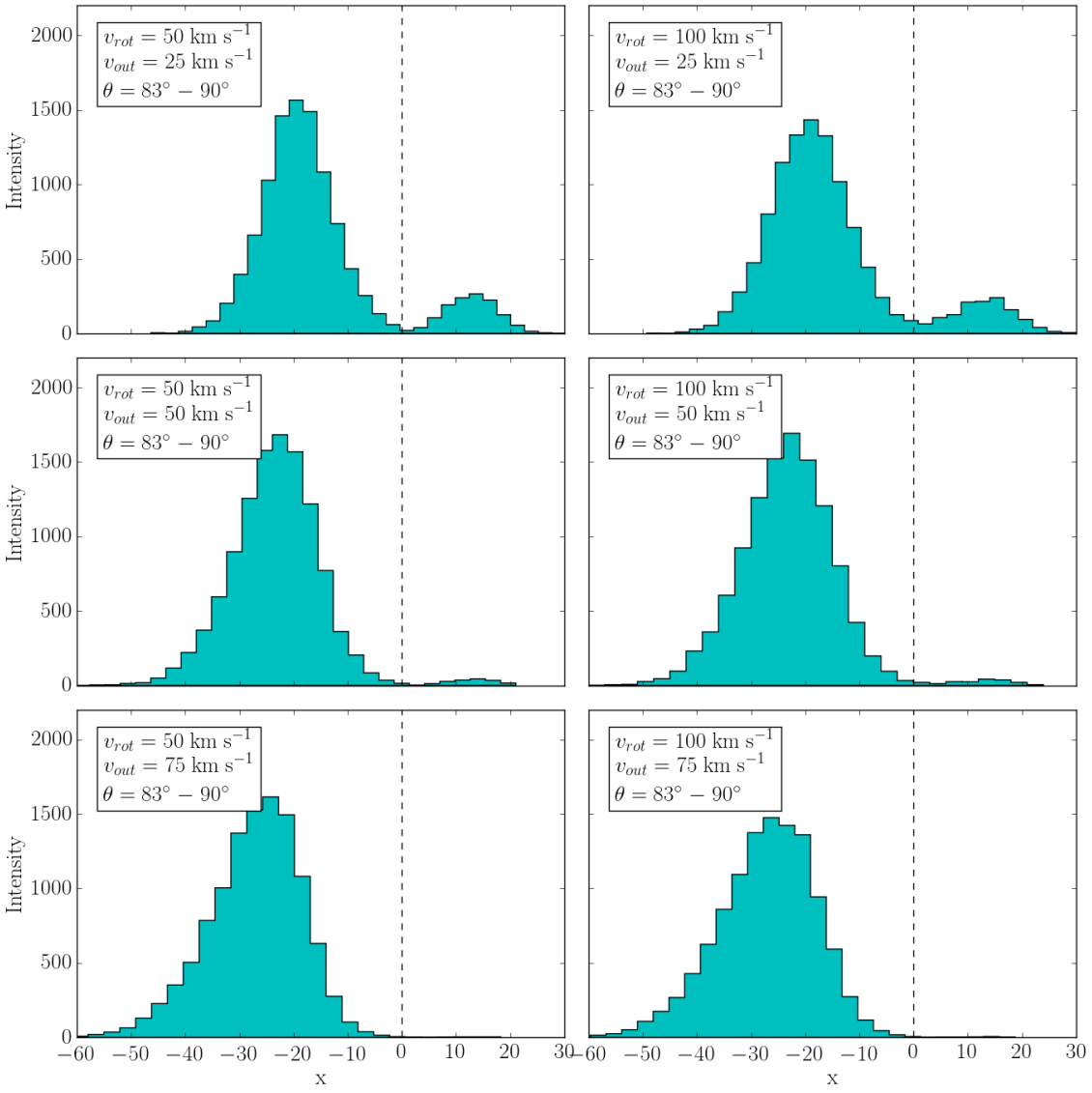

Figure 3.7: **Ly-α profile for $\tau_{\rm H} = 10^5$:** With $v_{\rm rot}$ ranging $50, 100$ km s^{-1}and $v_{\rm out}$ ranging $25, 50, 75$ km s^{-1}.

In these three sets of figures (Fig. 3.5 3.6 3.7) we can now see a clear second peak in more histograms. However when $v_{\rm out}$ / $v_{\rm rot} \geq 1$ the effect is negligible and can't still fully appreciate the rotation impact in the line. For this reason we had to run a 3rd set of parameters with $v_{\rm out}$ much smaller now.

3.2.3 3rd run

In this run we took v_{out} below the lowest v_{out} of the 2nd run, but still the same v_{rot} as before. However as the magnitude of the velocity is now smaller, we did not run $\tau_{\text{H}} = 10^7$ because it wouldn't be consistent with it.

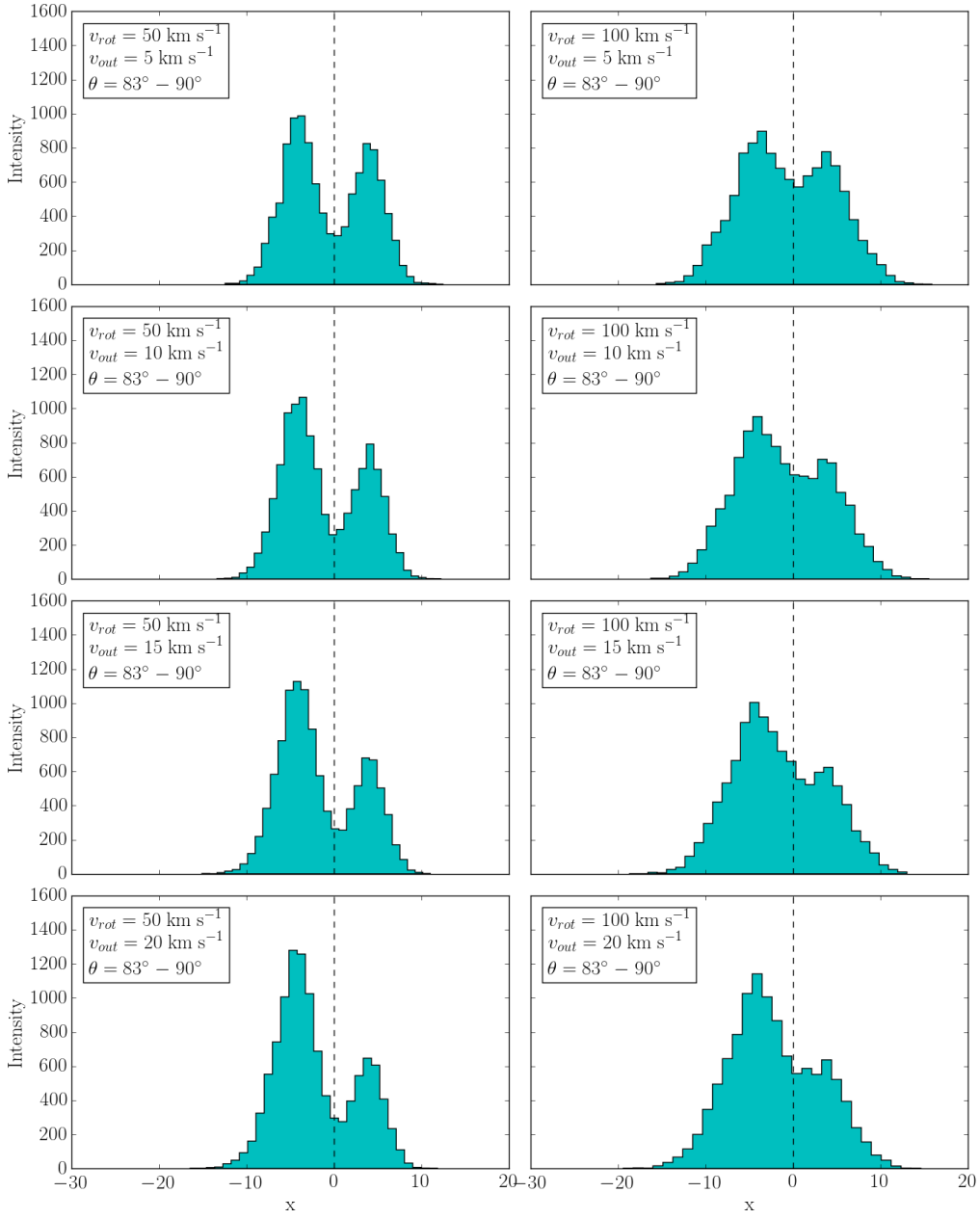

Figure 3.8: **Ly-α profile for $\tau_{\text{H}} = 10^5$:** With v_{rot} ranging $50, 100$ km s^{-1}and v_{out} ranging $5, 10, 15, 20$ km s^{-1}.

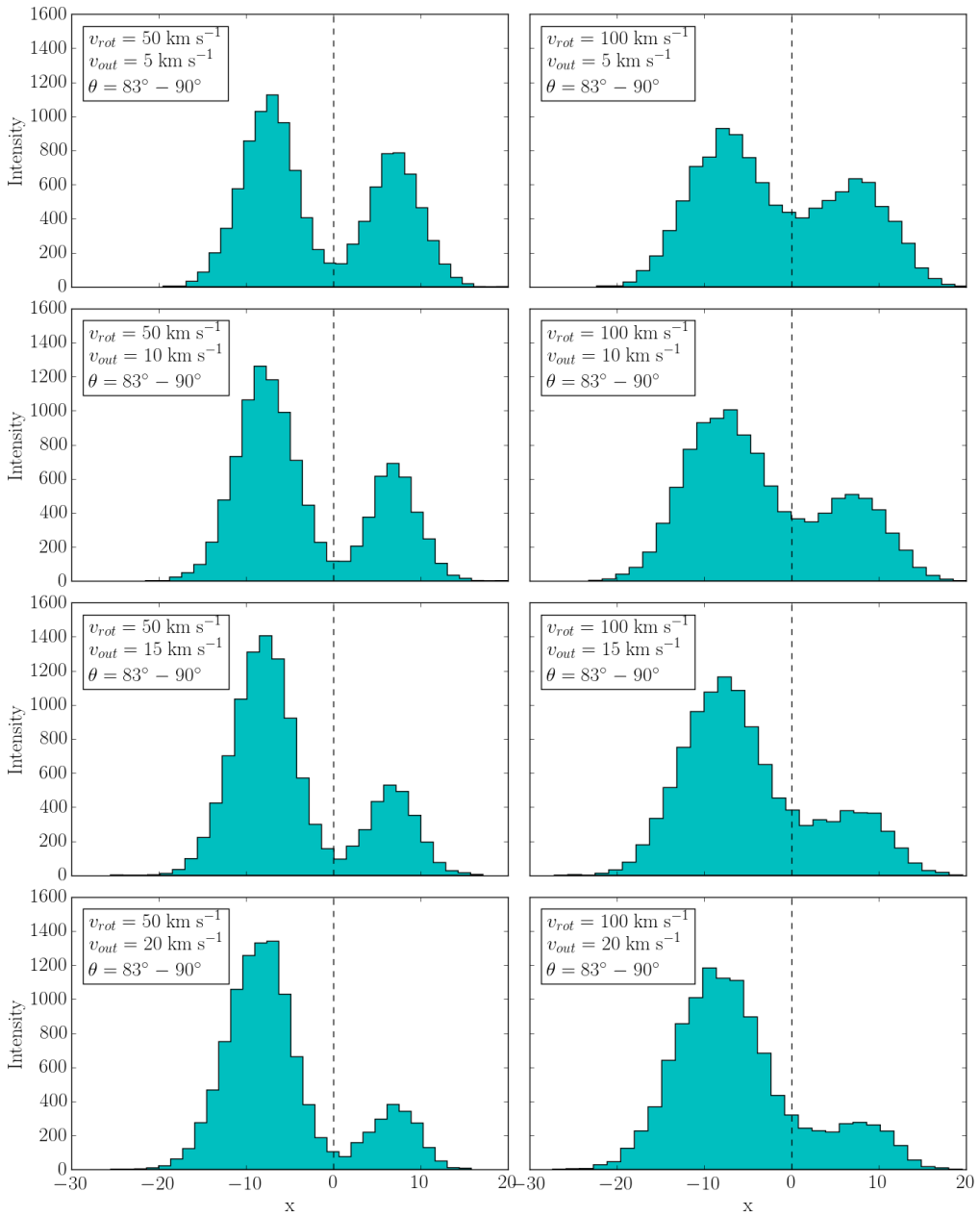

Figure 3.9: **Ly-α profile for $\tau_{\mathrm{H}} = 10^6$:** With v_{rot} ranging $50, 100$ km s^{-1}and v_{out} ranging $5, 10, 15, 20$ km s^{-1}.

These combinations of values make a lot more sense if we recall that v_{out} is caused mainly by starbursts, ejection of material out the galaxy. For this is not common that a galaxy expands faster than it rotates and from the figures (Fig. 3.8 3.9) we can confirm that only a little fraction of the v_{rot} radially is necessary to obtain 2 asymmetric peaks.

3.3 Morphology of Ly-α line

From now on, we will only show the results based on the 3rd run parameters combinations. In this section we will measure with 3 different quantities, the morphology of the Ly-α line in dependence of the velocities. First, we will use the standard deviation (std), then the skewness (skw) and finally a factor sigma of asymmetry (σ_A) defined by (MISSING REFERENCE).

3.3.1 Standard Deviation

In this part we will use the std to estimate the dispersion of the frequencies in the Ly-α line. Is important to recall that if the value is close to zero, then the frequencies tend to be very close to their expected value. If it increases, it means the frequencies are spreading to wider ranges.

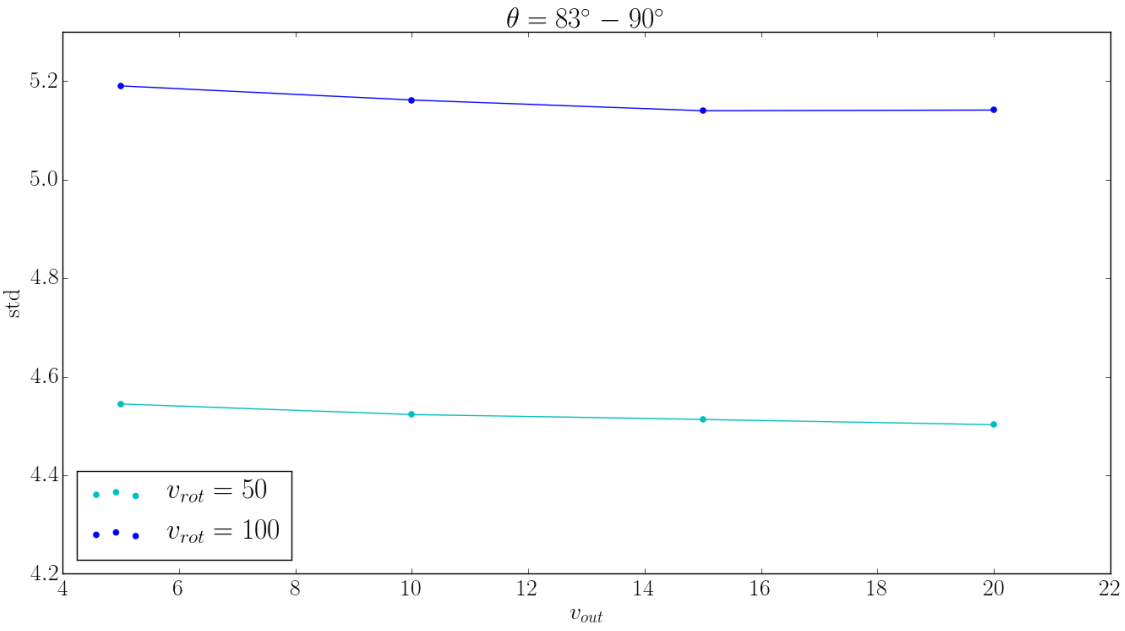

Figure 3.10: **Skewness plot for $\tau_{\mathrm{H}} = 10^5$.**

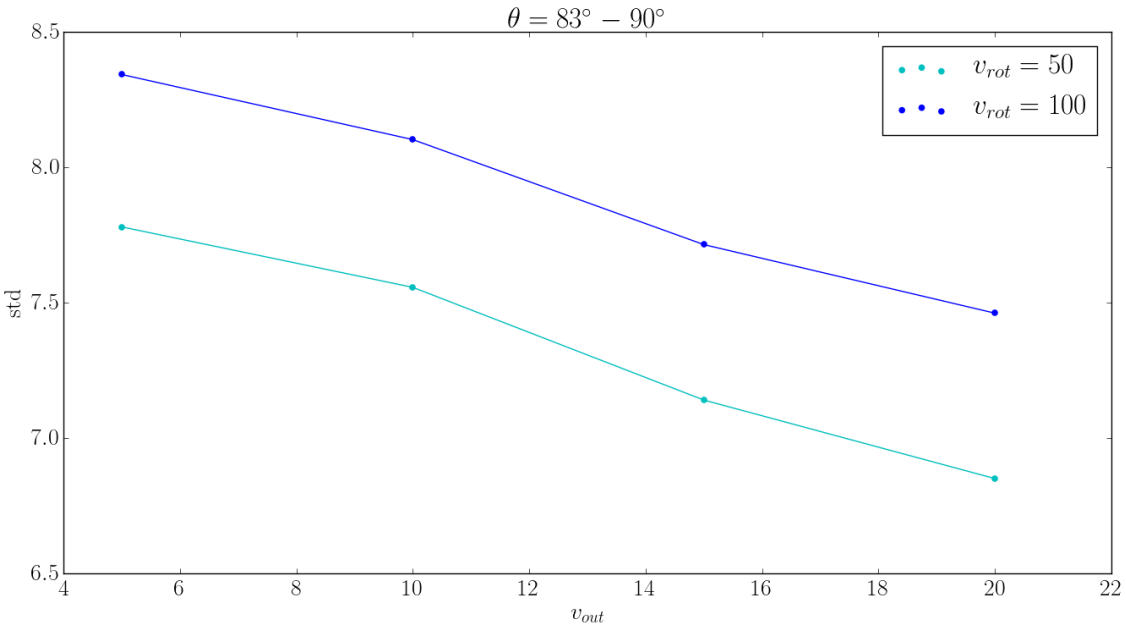

Figure 3.11: **Skewness plot for $\tau_{\mathrm{H}} = 10^6$.**

As seen in figures (Fig. 3.10 3.11), the standard deviation is inversely proportional to the outflow velocity. And the higher the τ_{H} , the more inclined the curves. This implies that the greater v_{out} is, the less disperse the Ly-α frequency distribution. This clearly shows that the peaks start merging to one another it v_{out} is increasing.

3.3.2 Skewness

In this part we will use the skw to estimate the asymmetry of the Ly-α line. Is important to recall that if the value is greater than zero, there is more weight in the left tail of the line. And on the contrary, if it is less than zero, there is more weight in the right one.

As seen in figures (Fig. 3.12 3.13), the skewness is proportional to the outflow velocity. This implies that the greater v_{out} is, the more asymmetric is the Ly-α frequency distribution.

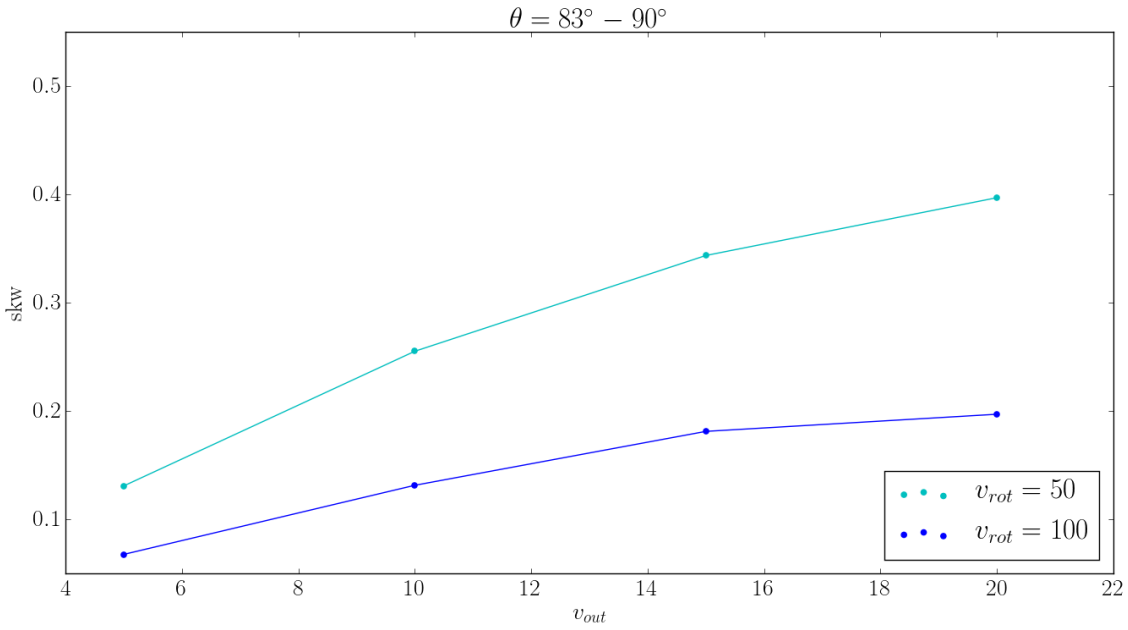

Figure 3.12: **Skewness plot for $\tau_{\mathrm{H}} = 10^5$.**

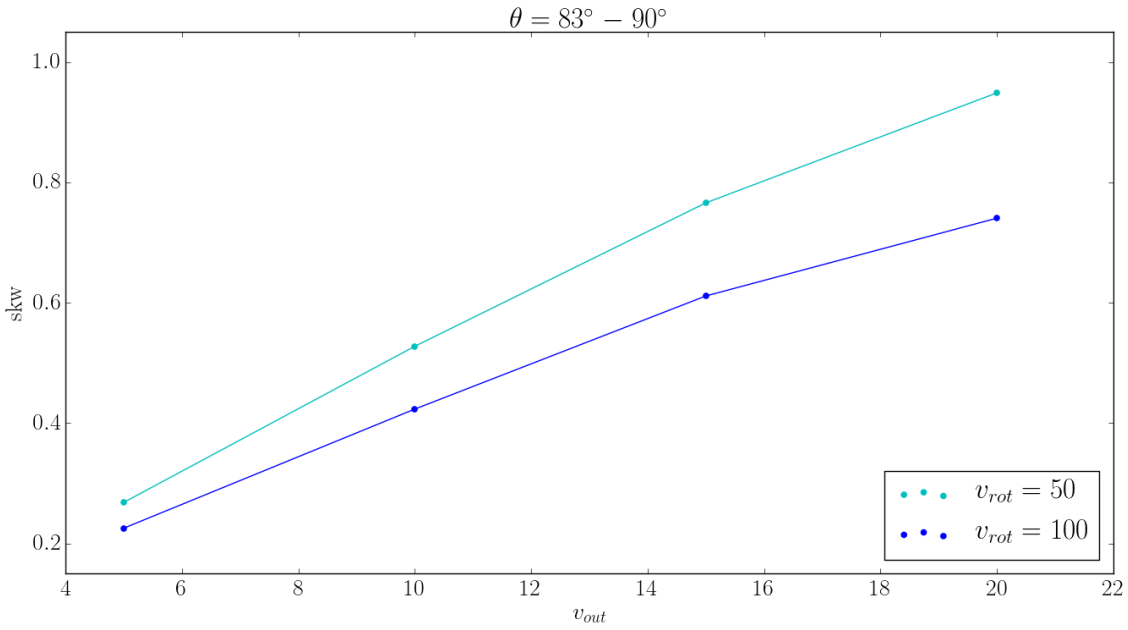

Figure 3.13: **Skewness plot for $\tau_{\mathrm{H}} = 10^6$.**

3.3.3 Sigma of Asymmetry

In this part we will use the σ_A factor to estimate in another way the asymmetry of the Ly-α line. This was defined by (MISSING REFERENCE) as follows. The two peaks, the left one and the right one, are fitted with a Gaussian curve and their

standard deviations σ_{left} and σ_{right} are obtained. Then the factor σ_A is:

$$\sigma_A = \frac{\sigma_{right}}{\sigma_{left}} \tag{3.3.1}$$

Is important to recall that if the value is greater than one, the left peak is thiner than the right peak. And if it is less than one, there left peak is wider than the right peak.

(MISSING PLOT)

3.4 Influences of the free parameters

3.4.1 Influence of the Galaxy Rotation Velocity: $v_{\rm rot}$

The influence of $v_{\rm rot}$ is slightly clear because of the giant impact $v_{\rm out}$ has. However it is noticeable that the Ly-α line broadens and lowers intensity when the rotation velocity increases. This result is consistent with Garavito et al. [33].

3.4.2 Influence of the Galaxy Outflow Velocity: $v_{\rm out}$

The influence of $v_{\rm out}$ is very clear since the first run. When this outflows velocity increases, the right peak of the spectrum goes down in intensity until it merges with the left peak.

3.4.3 Influence of the Galaxy Optical Depth: $\tau_{\rm H}$

The influence of $\tau_{\rm H}$ in the Ly-α line can be seen clearly in figures (Fig. 3.2 3.3 3.4). What the optical depth causes is that the more $\tau_{\rm H}$ there is, the more redshifted is the line respect to the zero value.

Chapter 4

Discussion

TO ADD:

- Comparison with some other result (probably observations).

- Why is this result useful?

- What possible implications can this model have?

Chapter 5

Conclusions

Here goes the conclusions....

Chapter 6

Bibliography

[1] Fernando Pérez and Brian E. Granger. Ipython: a system for interactive scientific computing. *Computing in Science and Engineering*, 9(3):21–29, May 2007.

[2] J. D. Hunter. Matplotlib: A 2d graphics environment. *Computing In Science & Engineering*, 9(3):90–95, 2007.

[3] R. B. Partridge and P. J. E. Peebles. Are Young Galaxies Visible? *ApJ*, 147:868, March 1967.

[4] S. Djorgovski and D. J. Thompson. Searches for Primeval Galaxies. In B. Barbuy and A. Renzini, editors, *The Stellar Populations of Galaxies*, volume 149 of *IAU Symposium*, page 337, 1992.

[5] J. E. Rhoads, S. Malhotra, A. Dey, D. Stern, H. Spinrad, and B. T. Jannuzi. First Results from the Large-Area Lyman Alpha Survey. *ApJl*, 545:L85–L88, December 2000.

[6] E. Gawiser, H. Francke, K. Lai, K. Schawinski, C. Gronwall, R. Ciardullo, R. Quadri, A. Orsi, L. F. Barrientos, G. A. Blanc, G. Fazio, and J. J. Feldmeier. Lyα-Emitting Galaxies at z = 3.1: L* Progenitors Experiencing Rapid Star Formation. *ApJ*, 671:278–284, December 2007.

[7] R. S. Koehler, P. Schuecker, and K. Gebhardt. Probing dark energy with baryonic acoustic oscillations at high redshifts. *A&A*, 462:7–20, January 2007.

[8] M. Ouchi, K. Shimasaku, M. Akiyama, C. Simpson, T. Saito, Y. Ueda, H. Furusawa, K. Sekiguchi, T. Yamada, T. Kodama, N. Kashikawa, S. Okamura, M. Iye, T. Takata, M. Yoshida, and M. Yoshida. The Subaru/XMM-Newton Deep Survey (SXDS). IV. Evolution of Lyα Emitters from z=3.1 to 5.7 in the 1 deg^2 Field: Luminosity Functions and AGN. *ApJs*, 176:301–330, June 2008.

[9] T. Yamada, Y. Nakamura, Y. Matsuda, T. Hayashino, R. Yamauchi, N. Morimoto, K. Kousai, and M. Umemura. Panoramic Survey of Lyα Emitters at z = 3.1. *AJ*, 143:79, April 2012.

[10] M. A. Schenker, D. P. Stark, R. S. Ellis, B. E. Robertson, J. S. Dunlop, R. J. McLure, J.-P. Kneib, and J. Richard. Keck Spectroscopy of Faint 3 z 8 Lyman Break Galaxies: Evidence for a Declining Fraction of Emission Line Sources in the Redshift Range 6 z 8. *ApJ*, 744:179, January 2012.

[11] K. R. Kulas, A. E. Shapley, J. A. Kollmeier, Z. Zheng, C. C. Steidel, and K. N. Hainline. The Kinematics of Multiple-peaked Lyα Emission in Star-forming Galaxies at z ˜ 2-3. *ApJ*, 745:33, January 2012.

[12] T. S. Chonis, G. A. Blanc, G. J. Hill, J. J. Adams, S. L. Finkelstein, K. Gebhardt, J. A. Kollmeier, R. Ciardullo, N. Drory, C. Gronwall, A. Hagen, R. A. Overzier, M. Song, and G. R. Zeimann. The Spectrally Resolved Lyα Emission of Three Lyα-selected Field Galaxies at z ˜ 2.4 from the HETDEX Pilot Survey. *ApJ*, 775:99, October 2013.

[13] S. L. Finkelstein, C. Papovich, M. Dickinson, M. Song, V. Tilvi, a. M. Koekemoer, K. D. Finkelstein, B. Mobasher, H. C. Ferguson, M. Giavalisco, N. Reddy, M. L. N. Ashby, a. Dekel, G. G. Fazio, a. Fontana, N. a. Grogin, J.-S. Huang, D. Kocevski, M. Rafelski, B. J. Weiner, and S. P. Willner. A galaxy rapidly forming stars 700 million years after the Big Bang at redshift 7.51. *Nature*, 502(7472):524–527, October 2013.

[14] G. Östlin, M. Hayes, F. Duval, A. Sandberg, T. Rivera-Thorsen, T. Marquart, I. Orlitova, A. Adamo, J. Melinder, L. Guaita, H. Atek, J. M. Cannon, P. Gruyters, E. C. Herenz, D. Kunth, P. Laursen, J. M. Mas-Hesse, G. Micheva,

H. O.-F. S. A. Pardy, M. M. Roth, D. Schaerer, and A. Verhamme. The Lyman-alpha Reference Sample: I. Survey outline and first results for Markarian 259. *ArXiv e-prints*, September 2014.

[15] M. Hayes, G. Östlin, F. Duval, A. Sandberg, L. Guaita, J. Melinder, A. Adamo, D. Schaerer, A. Verhamme, I. Orlitová, J. M. Mas-Hesse, J. M. Cannon, H. Atek, D. Kunth, P. Laursen, H. Otí-Floranes, S. Pardy, T. Rivera-Thorsen, and E. C. Herenz. The Lyman Alpha Reference Sample. II. Hubble Space Telescope Imaging Results, Integrated Properties, and Trends. *ApJ*, 782:6, February 2014.

[16] A. L. Faisst, P. Capak, C. M. Carollo, C. Scarlata, and N. Scoville. Spectroscopic Observation of Lyα Emitters at z ˜ 7.7 and Implications on Re-ionization. *ApJ*, 788:87, June 2014.

[17] M. Fumagalli, J. M. O'Meara, J. X. Prochaska, M. Rafelski, and N. Kanekar. Directly imaging damped Ly α galaxies at z 2 - III. The star formation rates of neutral gas reservoirs at z 2.7. $MNRAS, 446 : 3178 - -3198, January 2015$.

[18] M. Dijkstra. Lyman Alpha Emitting Galaxies as a Probe of Reionization. *ArXiv e-prints, arXiv:1406.7292*, June 2014.

[19] C. Behrens and J. Niemeyer. Effects of Lyman-alpha scattering in the IGM on clustering statistics of Lyman-alpha emitters. *A&A*, 556:A5, August 2013.

[20] M. Dijkstra and R. Kramer. Line transfer through clumpy, large-scale outflows: Ly α absorption and haloes around star-forming galaxies. *MNRAS*, 424:1672–1693, August 2012.

[21] M. Gronke, M. Dijkstra, M. Trenti, and S. Wyithe. Connecting Faint End Slopes of the Lyman-α emitter and Lyman-break Galaxy Luminosity Functions. *ArXiv e-prints*, January 2015.

[22] T. F. Adams. The Escape of Resonance-Line Radiation from Extremely Opaque Media. *ApJ*, 174:439, June 1972.

[23] J. P. Harrington. The scattering of resonance-line radiation in the limit of large optical depth. *MNRAS*, 162:43, 1973.

[24] D. A. Neufeld. The transfer of resonance-line radiation in static astrophysical media. *ApJ*, 350:216–241, February 1990.

[25] M. Dijkstra, Z. Haiman, and M. Spaans. Lyα Radiation from Collapsing Protogalaxies. I. Characteristics of the Emergent Spectrum. *ApJ*, 649:14–36, September 2006.

[26] P. Laursen, J. Sommer-Larsen, and A. C. Andersen. Lyα Radiative Transfer with Dust: Escape Fractions from Simulated High-Redshift Galaxies. *ApJ*, 704:1640–1656, October 2009.

[27] A. Verhamme, D. Schaerer, and A. Maselli. 3D Lyα radiation transfer. I. Understanding Lyα line profile morphologies. *A&A*, 460:397–413, December 2006.

[28] J. E. Forero-Romero, G. Yepes, S. Gottlöber, S. R. Knollmann, A. J. Cuesta, and F. Prada. CLARA's view on the escape fraction of Lyman α photons in high-redshift galaxies. *MNRAS*, 415:3666–3680, August 2011.

[29] M. Hansen and S. P. Oh. Lyman α radiative transfer in a multiphase medium. *MNRAS*, 367:979–1002, April 2006.

[30] S.-H. Ahn, H.-W. Lee, and H. M. Lee. P Cygni type Lyα from starburst galaxies. *MNRAS*, 340:863–869, April 2003.

[31] J. E. Forero-Romero, G. Yepes, S. Gottlöber, and F. Prada. Modelling the fraction of Lyman break galaxies with strong Lyman α emission at $5 \leq z \leq 7$. *MNRAS*, 419:952–958, January 2012.

[32] C. L. Martin, M. Dijkstra, A. Henry, K. T. Soto, C. W. Danforth, and J. Wong. The Lyα Line Profiles of Ultraluminous Infrared Galaxies: Fast Winds and Lyman Continuum Leakage. *ApJ*, 803:6, April 2015.

[33] J. N. Garavito-Camargo, J. E. Forero-Romero, and M. Dijkstra. The Impact of Gas Bulk Rotation on the Lyα Line. *ApJ*, 795:120, November 2014.

[34] D. A. Neufeld. The escape of Lyman-alpha radiation from a multiphase interstellar medium. *ApJl*, 370:L85–L88, April 1991.

[35] L. A. Barnes, M. G. Haehnelt, E. Tescari, and M. Viel. Galactic winds and extended Lyα emission from the host galaxies of high column density quasi-stellar object absorption systems. *MNRAS*, 416:1723–1738, September 2011.

[36] A. Verhamme, Y. Dubois, J. Blaizot, T. Garel, R. Bacon, J. Devriendt, B. Guiderdoni, and A. Slyz. Lyman-α emission properties of simulated galaxies: interstellar medium structure and inclination effects. *A&A*, 546:A111, October 2012.

[37] H. Yajima, Y. Li, Q. Zhu, T. Abel, C. Gronwall, and R. Ciardullo. Were Progenitors of Local L* Galaxies Lyα Emitters at High Redshift? *ApJ*, 754:118, August 2012.

[38] C. Behrens, M. Dijkstra, and J. C. Niemeyer. Beamed Lyα emission through outflow-driven cavities. *A&A*, 563:A77, March 2014.

[39] A. S. Chung, M. Dijkstra, B. Ciardi, and M. Gronke. Blue Wings and Bumps via Fermi-like Acceleration of Lyman-alpha photons across Shocks. *ArXiv e-prints*, September 2015.

[40] T. Hashimoto, A. Verhamme, M. Ouchi, K. Shimasaku, D. Schaerer, K. Nakajima, T. Shibuya, M. Rauch, Y. Ono, and R. Goto. A Close Comparison between Observed and Modeled Lyα Lines for z ˜ 2.2 Lyα Emitters. *ApJ*, 812:157, October 2015.

[41] M. Gronke, P. Bull, and M. Dijkstra. A Systematic Study of Lyman-α Transfer through Outflowing Shells: Model Parameter Estimation. *ApJ*, 812:123, October 2015.

[42] A. Orsi, C. G. Lacey, and C. M. Baugh. Can galactic outflows explain the properties of Ly α emitters? *MNRAS*, 425:87–115, September 2012.

[43] T. E. Rivera-Thorsen, M. Hayes, G. Östlin, F. Duval, I. Orlitová, A. Verhamme, J. M. Mas-Hesse, D. Schaerer, J. M. Cannon, H. Otí-Floranes, A. Sandberg, L. Guaita, A. Adamo, H. Atek, E. C. Herenz, D. Kunth, P. Laursen, and J. Melinder. The Lyman Alpha Reference Sample. V. The Impact of Neutral ISM Kinematics and Geometry on Lyα Escape. *ApJ*, 805:14, May 2015.

[44] B. Ryden and B. M. Peterson. *Foundations of Astrophysics.* 2010.

[45] S. Chandrasekhar. *Radiative transfer.* 1950.

[46] J. P. Walker-Soler, E. Gawiser, N. A. Bond, N. Padilla, and H. Francke. Present-day Descendants of z = 3 Lyα-emitting Galaxies in the Millennium-II Halo Merger Trees. *ApJ*, 752:160, June 2012.

[47] D. Narayanan, M. Bothwell, and R. Davé. Galaxy gas fractions at high redshift: the tension between observations and cosmological simulations. *MNRAS*, 426:1178–1184, October 2012.

[48] Planck Collaboration, P. A. R. Ade, N. Aghanim, M. Arnaud, M. Ashdown, J. Aumont, C. Baccigalupi, A. J. Banday, R. B. Barreiro, J. G. Bartlett, and et al. Planck 2015 results. XIII. Cosmological parameters. *ArXiv e-prints*, February 2015.

Appendix A

Rotation + Thin Shell Outflow

In this section we describe the two different models that together are used to reproduce a real and consistent Ly-α profile. The first one is a rotation model for the galaxy and the second is a thin shell model for the outflow.

A.1 Rotation Model

We use the simplified rotation model developed by [33] in which a rotating galaxy is modeled as a solid rotating sphere, with a homogeneous mixture of hydrogen and dust. Photons can be initially at the center or can be homogeneously distributed inside the sphere. The equations governing this solid-body rotation sphere in which the axis of rotation is defined to be align with the z-axis are:

$$v_x = -\frac{y}{R} V_{\max}, \tag{A.1.1}$$

$$v_y = \frac{x}{R} V_{\max}, \tag{A.1.2}$$

$$v_z = 0, \tag{A.1.3}$$

Where R is the radius of the sphere and $V_{\max}$ is the linear velocity at the sphere's surface. The minus/plus sign in the x/y-component of the velocity indicates the direction of rotation. In this case we take the angular velocity in the same direction as the $\hat{k}$ unit vector.

In this work we use the analytical expression for rotation derived in [33] where a rotating sphere can be seen as a static sphere in the laboratory frame with a bulk velocity difference in each surface element with respect to a distant observer. With the previous analysis the outcoming spectra can be expressed as:

$$J(x,i) \approx 2\pi \int_0^R db\, b \int_0^{2\pi} d\phi\, J(x,b,\phi,i), \tag{A.1.4}$$

Where $J(x,b,\phi,i)$ is the spectrum of the flux emerging from the surface at point (b,ϕ) and is expressed as:

$$J(x,b,\phi,i) = \frac{\sqrt{\pi}}{\sqrt{24}a\tau_0}\left(\frac{(x-x_{\rm b})^2}{1+\cosh\left[\sqrt{\frac{2\pi^3}{27}}\frac{|(x-x_{\rm b})^3|}{a\tau_0}\right]}\right) \tag{A.1.5}$$

A.2 Thin Shell Outflow Model

We use an outflow model that follows the characteristics put described in [27] with the code presented in [42]. The outflow consists of an isothermal, spherical flow expanding at constant velocity $v_{\rm out}$. The outflow is empty inside the shell's inner radius R_{in} and reaches out to an external radius R_{out}. The relationship between these two radii is parameterized by $R_{in} = f_{th}R_{out}$, with $f_{th} = 0.9$ as the fiducial value. The temperature of the medium is assumed constant and equal to $T = 10^4 K$

which sets the velocity dispersion of Maxwell-Boltzmann distributions to $v_{\rm th} = 12.84$ km s^{-1}.

The gas has an homogeneous Hydrogen number density inside the flow. The total mass inside the shell is parameterized by its column density

$$N_H = \frac{X_H M_{shell}}{4\pi m_H R^2{}_{out}}, \tag{A.2.6}$$

where M_{shell} is the outflow mass, m_H is the mass of the hydrogen atom and $X_H = 0.74$ is the fraction of hydrogen in the cold gas.

The outflow also includes dust homogeneously mixed with the gas. The dust optical depth τ_d is parameterized by the metallicity of the cold gas $\langle Z_{cold} \rangle$:

$$\tau_d ???? \langle Z_{cold} \rangle \tag{A.2.7}$$

A.3 Joint Model

The joint model consists of combining the two models that were just explained. A rotating spherical galaxy is placed at the center with a thin shell outflow surrounding it as seen in Fig. A.1. What happens is that the photons that escaped the galaxy enter now into the outflow with the same radial direction that they came out with. At the end only a fraction of those manage to get out of the outflow and their wavelengths are measured to find the final spectrum.

In order to simulate all the possible cases we set some key parameters for the program to vary, and some others fixed which are defined by the characteristics of LAEs. This are chosen as follows.

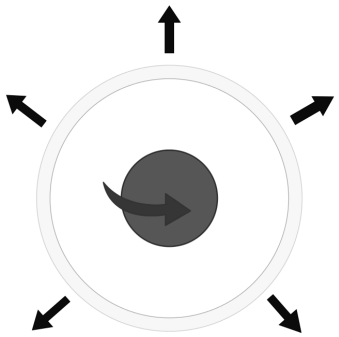

Figure A.1: **Model:** A central rotating galaxy surrounded by an expanding thin shell outflow.

A.4 Galaxy Parameters

Our aim is to provide a realistic baseline to compare against observations of LAES at $z \sim 3$. It has been found by analysis of the abundance and angular correlation function that LAES reside in DM halos of masses in the range $10^{10} - 10^{11}\mathrm{M}_{\odot}$[46]. This mass range corresponds to maximum circular velocities in the range $60 - 125\,\mathrm{km\ s^{-1}}$and a median halo scale radius of 15kpc. [1].

These galaxies have gas fractions close to 20% ([47]). We approximate that the hydrogen content is 20% the total baryonic content from the cosmological baryon to dark matter abundances $\Omega_b/\Omega_{dm} = 0.1825$ ([48]), multiplied by a primordial Hydrogen fraction of 0.75. All these considerations gives us hydrogen masses in the range $2.7 \times 10^8 - 2.7 \times 10^9\mathrm{M}_{\odot}$.

These choices give us a range for the number density of Hydrogen atoms of $4 \times 10^{-4} - 4 \times 10^{-3}$ atoms cm^{-3}. With a Lyman-α cross section at the line center of $\sigma_H = 1.0 \times 10^{-14}$ cm^2 we finally obtain that the optical depth from the cloud's center should be in the range $\tau = 2 \times 10^5 - 2 \times 10^6$.

[1] These results were found using the N-body data available in `www.cosmosim.org`

From these constraints we chose to model two kinds of central galaxies in the extremes of these distributions. The first has $\tau = 2 \times 10^5$ and a raotational velocity of 60 km s^{-1}. The second has $\tau = 2 \times 10^6$ and a rotational velocity of 125 km s^{-1}.

For the first stage there are two fixed parameters: the optical depth $\tau = 10^8$ and the galaxy viewing angle $\theta_{gal} = 90°$. For the second stage there is one fixed parameter: the metallicity of the outflow $Z = -4.0$. This 3 fixed values are selected because the characteristics of observed LAEs, especially their low mass and their highest star formation rate of all.

We have then 3 parameters left that are going to vary along a wide range. These are: the galaxy rotation velocity $v_{\rm rot}$, the outflow hydrogen column density n_H and the outflow expanding velocity $v_{\rm out}$.

$v_{\rm rot}$ covers 3 different angles: 20 km s^{-1}, 100 km s^{-1}and 200 km s^{-1}. $\log n_H$ takes 41 different values from 20.0 to 22.5. And $v_{\rm out}$ covers 5 equidistant velocities from 100 km s^{-1}to 500 km s^{-1}.

The results of this project consist of emulating a LAE spectrum basing on its physical characteristics defined by the 3 free parameters we stated before. When defined the combination of those three.

In the following section each free parameter is explained deeper.

In order to study the influence of each of the three free parameters, we fix two of them and see how the final spectrum varies along the other one left. In each case we will state these changes.

A.4.1 Influence of the Galaxy Rotation Velocity: v_{rot}

If one sets fixed outflow v_{out} and $\log n_H$ in each case the rotation velocity has the same effect: it increases proportionally the intensities. However this change is not that significant. The resulting spectra are completely the same, but enlarged vertically by a small factor. Fig. A.2 helps visualize this effect in a better way.

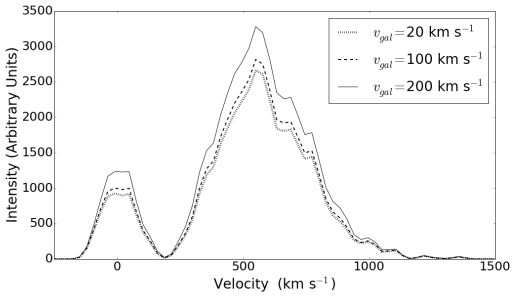

Figure A.2: **Influence of Galaxy Rotation Velocity:** The values of the fixed parameters are $v_{\mathrm{out}} = 100$ km s^{-1}and $\log n_H = 20.9375$. The 3 possible velocities are shown in the plot with different line styles. The increase is visible as well as its small enlargement factor.

A.4.2 Influence of the Outflow Hydrogen Column Density: $\log n_H$

The effect of the $\log n_H$ is the creation of 2 peaks: the left one very thin, tall and pronounced, and the right one very wide, small and soften. When the $\log n_H$ is increased, the left peak starts to decrease while mixing with the right one, decreasing their height ratio until the left peak completely disappears. The resulting spectrum, with high column density, is a wide single mountain with intensity significantly less than at the beginning. Fig. A.3 helps visualize this effect in a better way.

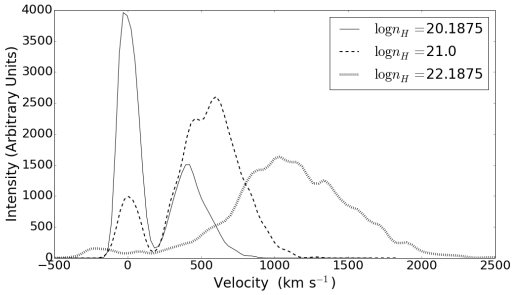

Figure A.3: **Influence of Outflow Hydrogen Column Density:** The values of the fixed parameters are $v_{\rm out} = 100$ km s^{-1}and $v_{\rm rot} = 100$ km s^{-1}. There are three stages of the $\log n_H$ value shown: initial, intermediate and final, with the values shown on the plot.

A.4.3 Influence of the Outflow Expanding Velocity: $v_{\rm out}$

The effect of this parameter consists in a shift of the initial spectrum in the column density. The more $v_{\rm out}$ the outflow has, the more the spectrum simulates the previous velocity but with a greater $\log n_H$. If one compares with Fig. A.3 the similarities are really clear.

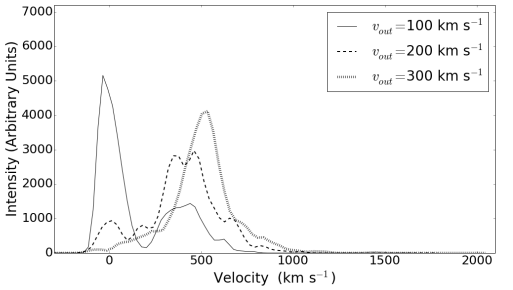

Figure A.4: **Influence of Outflow Expanding Velocity:** The values of the fixed parameters are $\log n_H = 20.125$ and $v_{\rm rot} = 100$ km s^{-1}.

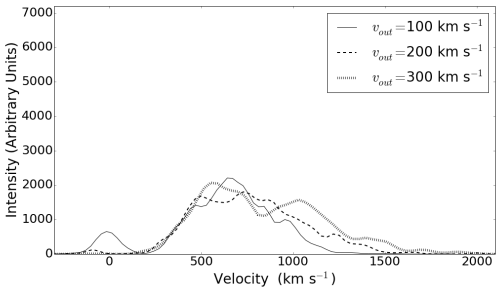

Figure A.5: **Influence of Outflow Expanding Velocity:** The values of the fixed parameters are $\log n_H = 21.25$ and $v_{\rm rot} = 100$ km s^{-1}.